Production of N_2O_5 and $ClNO_2$ through nocturnal processing of biomass-burning aerosol

Adam T. Ahern[1], Lexie Goldberger[2], Lydia Jahl[1], Joel Thornton[2], and Ryan C. Sullivan[1,*]
[1]Center for Atmospheric Particle Studies, Carnegie Mellon University
[2]Department of Atmospheric Science, University of Washington
*Corresponding Author: R.C. Sullivan (rsullivan@cmu.edu)

Abstract

Biomass burning is a source of both particulate chloride and nitrogen oxides, two important precursors for the formation of nitryl chloride ($ClNO_2$), a source of atmospheric oxidants that is poorly prescribed in atmospheric models. We investigated the ability of biomass burning to produce N_2O_5(g) and $ClNO_2$(g) through nocturnal chemistry using authentic biomass-burning emissions in a smog chamber. There was a positive relationship between the amount of $ClNO_2$ formed and the total amount of particulate chloride emitted, and with the chloride fraction of non-refractory particle mass. In every fuel tested dinitrogen pentoxide (N_2O_5) formed quickly following the addition of ozone to the smoke aerosol and $ClNO_2$(g) production promptly followed. At atmospherically relevant relative humidities, the particulate chloride in the biomass-burning aerosol was rapidly but incompletely displaced, likely by the nitric acid produced largely by the heterogeneous uptake of N_2O_5(g). Despite this chloride acid displacement, the biomass-burning aerosol still converted of order 10% of reacted N_2O_5(g) into $ClNO_2$(g). These experiments directly confirm that biomass burning is a potentially significant source of atmospheric N_2O_5 and $ClNO_2$ to the atmosphere.

TOC Art

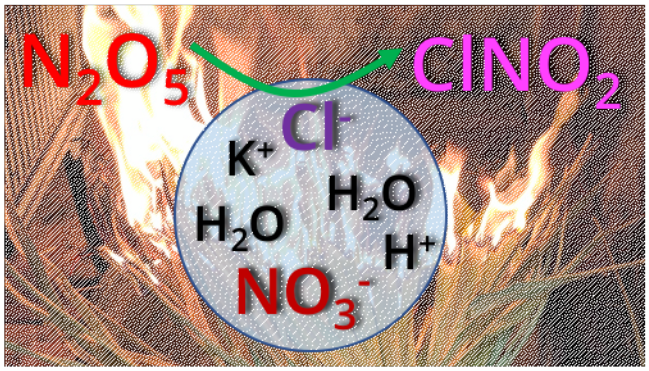

KEYWORDS: heterogeneous kinetics, photochemical smog, chemical ionization mass spectrometry, aerosol mass spectrometer, nitryl chloride, dinitrogen pentoxide, smog chamber reactor, biomass-burning smoke

1. Introduction

An accurate budget of atmospheric oxidants is necessary to predict the formation and loss of atmospheric pollutants and climate-forcing agents, such as methane and particulate matter. Atomic chlorine and nitrogen oxides (NO_x = NO + NO_2) are reactive gases that contribute significantly to the atmospheric oxidant budget, and whose lifetimes are directly impacted by the formation and fate of N_2O_5(g)[1,2]. N_2O_5 forms at night via reactions R1–R3, shown below. N_2O_5 is thermally unstable and exists in a temperature-dependent equilibrium with NO_2 + NO_3. At sunrise, NO_3 photolysis and its reaction with NO lead to rapid net loss of N_2O_5 back to NO_x [3–5].

$$\mathrm{NO} + \mathrm{O_3} \rightarrow \mathrm{NO_2} + \mathrm{O_2} \tag{R1}$$

$$\mathrm{NO_2} + \mathrm{O_3} \rightarrow \mathrm{NO_3} + \mathrm{O_2} \tag{R2}$$

$$\mathrm{NO_2} + \mathrm{NO_3} \underset{\Delta}{\leftrightarrow} \mathrm{N_2O_5} \tag{R3}$$

The N_2O_5 NO_x reservoir extends the atmospheric lifetime of the NO_x family by preventing removal through oxidation of NO_2 to HNO_3. N_2O_5 also reacts heterogeneously with aerosol particles [6]. The composition of the particle affects both the reactive uptake probability (γ_{N2O5}) and thus the rate of heterogeneous loss, and also the chemical fate of N_2O_5 that is taken up by the particle phase. N_2O_5 reacts in chloride containing aqueous particles to form either HNO_3(aq) or $ClNO_2$(aq)[7]. Reactions R4–R7 represent a hypothesized multi-step mechanism, though a concerted one-step process cannot be ruled out. The branching between the two products represents either net removal of two NO_x in the form of HNO_3, or the recycling of one NO_x and the formation of a Cl atom source: $ClNO_2$ [8,9].

$$\mathrm{N_2O_5}(g) \overset{K_4}{\leftrightarrow} \mathrm{N_2O_5}(aq) \tag{R4}$$

$$\mathrm{N_2O_5}(aq) + \mathrm{H_2O}(l) \overset{K_5}{\leftrightarrow} \mathrm{H_2ONO_2^+}(aq) + \mathrm{NO_3^-}(aq) \tag{R5}$$

$$\mathrm{H_2ONO_2^+}(aq) + \mathrm{H_2O}(l) \overset{k_6}{\rightarrow} \mathrm{HNO_3}(aq) + \mathrm{H_3O^+}(aq) \tag{R6}$$

$$\mathrm{H_2ONO_2^+}(aq) + \mathrm{Cl^-}(aq) \overset{k_7}{\rightarrow} \mathrm{ClNO_2}(aq) + \mathrm{H_2O}(l) \tag{R7}$$

$ClNO_2$ is formed in the particle phase, but then rapidly evaporates[8,9]. It is a stable gas in the dark, but quickly photo-dissociates into NO_2 and Cl·. Atomic chlorine is a radical of potency similar to the hydroxyl radical, and therefore affects the production of ozone, particulate matter, and hydroxyl radicals[10]. $ClNO_2$ has previously been observed in coastal regions where sea spray provides ample particulate chloride, a critical precursor to $ClNO_2$ formation[11,12]. However, elevated concentrations of $ClNO_2$ have recently been observed in a number of inland regions, suggesting the presence of other important but poorly understood reactive chlorine sources[13–17]. Production of $ClNO_2$ far from non-marine chloride sources represents a potentially important but uncertain perturbation to the atmospheric oxidant budget.

Biomass-burning aerosol (BBA) is a likely candidate source of chloride that leads to $ClNO_2$ formation because smoke plumes contain all the necessary precursors: NO_x, O_3, water, and often particulate chloride[18–20]. Analysis of a decade of measurements in the western US found a factor of 10 increase in PM chloride concentrations during wildfire smoke influenced periods.[21] The propensity for N_2O_5 to form in realistic biomass-burning plumes is not well known, and this is a prerequisite for the subsequent production of $ClNO_2$ [22]. Understanding biomass burning as a source of particulate chloride is of particular interest because it will allow us to better quantify $ClNO_2$ production from other more readily regulated chlorine sources such as coal burning power plants[14,23,24].

$ClNO_2$ production from biomass burning has yet to be investigated explicitly. In these experiments, we measured the $ClNO_2$ production potential of authentic BBA in smoke plume conditions. Although the formation of N_2O_5 is well understood, its heterogeneous uptake on authentic biomass-burning aerosol has not been explored through laboratory kinetics experiments. The two critical steps, reactive uptake of N_2O_5 (γ_{N2O5}) and the yield of $ClNO_2$ from N_2O_5 uptake (φ_{ClNO2}) are both highly dependent on particle composition and morphology[25–28]. The heterogeneous kinetics of authentic BBA, which varies in composition and morphology from particle to particle and depends on the type of fuel burned, may be significantly different from proxies used in previous lab studies[25,27,29–32]. The composition and morphology of BBA is difficult to predict because of the variability in sources, combustion conditions, and subsequent aging processes[18,33–37].

Three aerosol components are identified as having an important effect on the ability of particles to convert N_2O_5 into $ClNO_2$: water, nitrate, and chloride[7]. Even small mass fractions of aqueous particulate chloride may lead to the preferential formation of $ClNO_2$[7,8,38]. Kinetics experiments have found the ratio of k_7/k_6, R7/R6, is large (483±175)[7], favoring the formation of $ClNO_2$ instead of HNO_3 at chloride concentrations > 0.1 M in well-mixed aqueous inorganic solutions typical of atmospheric aerosol (e.g. ammonium-sulfate-nitrate systems)[7,8,39]. In contrast, aerosol nitrate, a product of N_2O_5 reactive uptake and dissolution of HNO_3 formed from gas-phase oxidation of NO_x [40], suppresses N_2O_5 reactive uptake via the so-called nitrate effect (reverse reaction in R5 equilibrium) [7,41]. In these experiments, we used biomass fuels with different anticipated chloride emissions (based on prior reports[18]) to investigate the effects of BBA chloride on $ClNO_2$ formation and to probe the relative competition between particle chloride and nitrate.

Water is also a critical component for the heterogeneous uptake of N_2O_5 and subsequent production of $ClNO_2$. Water is necessary to generate an aqueous phase to promote the efficient uptake of N_2O_5, and simultaneously dilutes the particle nitrate (thus enhancing γ_{N2O5}) and particle chloride (decreasing φ_{ClNO2}) concentrations[31,42]. Increased water content can also affect particle morphology (i.e. liquid-liquid phase separations[43–47]) and potentially facilitate net chloride displacement,[37,48] as shown in R8:

$$\mathrm{MCl}_{(\mathrm{s\ or\ aq})} + \mathrm{HNO}_{3(\mathrm{g})} \rightarrow \mathrm{HCl}_{(\mathrm{g})} + \mathrm{MNO}_{3(\mathrm{s\ or\ aq})} \qquad \text{(R8)}$$

where M is a cation (e.g. potassium, sodium, etc.). This mechanism can have the two-fold effect of increasing NO_3^- (thus decreasing γ_{N2O5}) and decreasing chloride (reducing φ_{ClNO2}), while releasing substantial HCl to the gas phase. In our smog chamber

experiments, we investigated the effect of relative humidity on the $ClNO_2$ produced from authentic BBA generated from various fuels that produced aerosol with a range of chloride contents to determine the influence of particle-phase water content on this multiphase chemistry.

2. Materials and Methods

2.1. Experimental overview

We investigated the fate of chloride in biomass-burning emissions in one of the Carnegie Mellon University 12 m^3 Teflon smog chambers[49,50]. A schematic of the chamber is shown in Figure 1. Prior to each experiment, the chambers were purged using UV blacklights and VOC-free and particle-free air overnight to ensure the particle number concentrations were < 10 cm^{-3}. We used four types of aerosol in these experiments. Ammonium bisulfate was selected as a test particle that did not contain chloride and that has a well-characterized γ_{N2O5} value[7,25,31]. The three biomass fuels burned were sawgrass, cutgrass, and birch wood. Sawgrass and cutgrass smoke have previously been observed to have high-chloride content, likely due to the brackish water they grow in[19]. These tall grasses were obtained for us from near Savannah, Georgia by the U.S. Fish and Wildlife Service, while the birch was bought as firewood at a local grocery store in Pittsburgh, PA. Information on the prevalence of these fuels in the United States, their chloride emission factors[18,51], and their fire and prescribed burn frequencies[52] is provided in the Supporting Information.

We prepared a 1 g L^{-1} solution of ammonium bisulfate in MilliQ water that we nebulized directly into the smog chamber using a TSI model 3076 aerosol generator. In some experiments the aerosol was passed through a diffusion drier, and in others the aerosol remained deliquesced before being injected into the pre-humidified smog chamber. We scattered tall grass samples in an aluminum pan and ignited them using a butane lighter. We added fuel by hand to maintain visual flaming combustion conditions while we filled the smog chamber using a pair of Dekati eductor dilutors[53]. We used the same sampling set up for the birch-wood smoke, except that the birch wood was burned in a naturally aspirated cast-iron woodstove with the door left open. It was allowed to burn for about 5 minutes before chamber filling was started. The fires were fed until the smog chamber contained a sufficient particle concentration. We aimed for a particle surface area concentration of ~2 x 10^9 nm^2 cm^{-3}, which was typically achieved after 20 to 40 minutes of particle injection. This corresponded to a particle number concentration of 3.5x10^5 cm^{-3} which decreased as particles diffused to the walls to an average number concentration of 2.0 x 10^5 cm^{-3} over 1.7 hours, but varied significantly for each experiment. The technical details of the sampling apparatus and the artefacts associated with sampling the naturally aspirated smoke are discussed in the Supplemental Information, along with details for each experiment provided in Table S1.

N_2O_5 was formed in the smoke by injecting ozone generated from pure oxygen gas flowing through a corona discharge source (HTU500AC, Azco) to the NO_x rich smoke and allowing reactions R1–R3 to occur in the chamber. Initial ozone concentrations were typically 95 ppbv. During our experiments, the smoke injection increased the chamber concentration of NO_x to an average concentration of 72 ppbv, as indicated in Table S1.

For experiments where smoke was not used, small aliquots (~1.2 mL) of 1% NO_2 (Liquid Technologies, Co.) were added to the chamber prior to ozone injection to achieve NO_x levels similar to those obtained in the burn experiments.

As the conversion of N_2O_5 into $ClNO_2$ is understood to occur in the aqueous phase, we also explored the effect of relative humidity on $ClNO_2$ formation. We achieved a relative humidity as high as 60% with minimal air dilution by injecting steam into the smog chamber. We heated approximately 300 mL of MilliQ water in a 3-neck 500 mL glass flask using an electric mantle[54]. Additional experimental details are described in the Supporting Information.

2.2. Particle characterization

We measured particle composition using the Aerodyne Soot Particle high resolution Aerosol Mass Spectrometer (SP-AMS, Aerodyne Research Inc.)[55]. The SP-AMS uses a high-power infrared (IR) laser to evaporate black-carbon containing aerosol, facilitating the measurement of refractory black carbon (rBC) aerosol mass by the AMS. Particles that do not contain rBC – and therefore do not efficiently absorb the IR laser – are evaporated by the conventional 600 °C tungsten thermal vaporizer that sits behind the IR laser beam. The vapors produced by either the IR laser or vaporizer are subsequently ionized by a 70 eV electron source, and the resulting ions are analyzed by a high-resolution time-of-flight mass spectrometer. Unless specified otherwise, refractory species were measured with the SP-AMS infrared (IR) laser on, using particle beam-width probe measurements to estimate the rBC collection efficiency ($E_{IR,rBC} = 0.4 \pm 0.15$)[56,57]. Due to uncertainty associated with the relative ionization efficiencies of non-refractory species vaporized with the SP-AMS using the IR laser, we report non-refractory species as measured when only using the conventional 600 °C vaporizer with the IR laser off[56–60]. The chloride salts present in BBA are typically KCl and NH_4Cl[18,61], which are non-refractory at 600 °C, unlike NaCl. With the conventional vaporizer, the largest source of uncertainty for quantitative mass measurements is caused by particles bouncing off the vaporizer and thus being undetected[62,63]. However, with biomass-burning aerosol there are assumptions that allow us to estimate particle bounce by comparing SP-AMS mass measurements with the laser on versus laser off. Further details on the SP-AMS data analysis procedures are provided in the Supporting Information.

We measured particle size and number using a Scanning Mobility Particle Sizer (SMPS, TSI, Inc., model 3081; 3080 long DMA and 3772 CPC) equipped with a polonium neutralizer, sampling directly from the chamber. The SMPS sheath flow was set to 5.0 L min^{-1} and the aerosol sample flow was reduced to 0.5 L min^{-1} using a mass flow controller to supply a particle-free makeup flow for the CPC's 1.0 L min^{-1} total flow rate. We calculated the particle surface area assuming all particles are spherical.

2.3. Gas-phase characterization

We measured the gas-phase composition using an absorption-based ozone monitor (Dasibi, 1008-PC), a chemiluminescence NO_x monitor with a molybdenum catalyst (Advanced Pollution Instrumentation, model 200A), and a relative humidity

probe (Vaisala, HNP-233). It should be noted that the NO_x data will be biased high due to unconstrained conversions of nitrogen oxides (e.g. N_2O_5) to NO[64,65]. At most this would bias NO_x 10% high, and would not influence our results significantly.

We measured iodide-ion adducts of N_2O_5 and $ClNO_2$ using the University of Washington high-resolution chemical ionization time of flight mass spectrometer (UW-CIMS)[39,66,67]. The UW-CIMS pulled 8.0 Lpm of flow through a 3/8″ o.d. Teflon sampling inlet to limit the loss of reactive and semi-volatile species. Laminar flow was calculated for these conditions with a 15% loss rate to the walls to limit the loss of reactive gases. A ^{210}Po ionizer (Staticmaster, model P-2021) was used to create reagent ions (I^-) from methyl iodide. The mass spectrometer was tuned for weak declustering and N_2O_5 and $ClNO_2$ were detected as clusters with the iodide ion. The inlet and ion molecule reaction region was humidified to a minimum of 35% RH to control for variable sensitivity to water vapor of target compounds[68].

The CIMS was calibrated using an online continuous source of N_2O_5 generated from the reaction of NO_2 and O_3, as described in Bertram et al.[69]. The source output has been checked against NO_x, O_3, and NO_y instruments and found to be stable for consistent inputs of NO_2 and O_3. Moreover, the instrument response to N_2O_5 derived from these additions is compared to the theoretical response, based on collision limited ionization and found to be consistent with expectations as described in Lopez-Hilfiker et al.[70].

We quantified the loss of N_2O_5 in the inlet using an N_2O_5 source placed in front of the inlet, similar in principle to that described by Bertram et al.[69], to generate a constant flowing concentration of N_2O_5 by reacting a stream of NO_2 with an excess of O_3. A dynamic gas-calibrator (Thermo Electron Co., model 146C) supplied a variable flow of NO from a compressed-gas cylinder (1500 ppb NO, Liquid Technologies Co.) and also generated a constant flow of O_3 from compressed zero air. We used a passivated 4 L glass bottle reservoir to allow ample reaction time for the NO_2 and O_3 to generate a steady source of N_2O_5. $ClNO_2$ was calibrated by flowing N_2O_5 over a saturated NaCl(aq) bed and assuming complete conversion from N_2O_5 to $ClNO_2$ [39].

3. Results and Discussion

3.1. Particle composition from biomass burning

We list the initial particle composition for each chamber experiment in Table S1, including the chloride fraction of non-refractory aerosol mass (*fCl* = Cl^- / (Cl^- + NO_3^- + organics + NH_4^+ + SO_4^{2-})). In these calculations we assume that all chloride is non-refractory, although thermodenuder studies of BBA have shown that as much as 10% can be semi-refractory,[71] and thus our *fCl* reported may be a slight under prediction. The initial particle composition of the smoke varied from burn-to-burn but there were some trends based on the fuel burned. Burning sawgrass produced the aerosol with the highest *fCl*, 0.32. Burning cutgrass could also generate high *fCl* aerosol, but in one instance had a very low *fCl* of 0.03. Birch-wood smoke consistently had the lowest chloride content with *fCl* = 0.01, with one exception where *fCl* = 0.09. It should be noted however, that although the birch wood had low chloride content, other parts of the plant that we did not burn may have contained elevated chloride concentrations. The chloride-enriched greens of

trees, which are readily burned in wildfires, can produce higher concentrations of chloride when burned than the lignin-rich wood[72,73]. This upper limit of *fCl* ~30% is in good agreement with the highest reported *fCl* by Levin et al. who analyzed fresh BBA from a variety of fuels[18]. Ambient measurements of aged smoke thought to be influenced by biomass burning report lower *fCl* values of less than 1%[74]. However, this aged aerosol was mixed with non-BBA, and had experienced significant chemical and photochemical processing, including the displacement of HCl by HNO_3 and H_2SO_4[61]. In addition to particle composition, Table S1 also lists the relative humidity in the chamber at the time of the aerosol measurement. The effects of relative humidity will be discussed in greater detail in the context of the gas-phase measurements in Section 3.3.

3.2. Production of N_2O_5 and $ClNO_2$ in biomass-burning smoke

N_2O_5 was produced rapidly in all our biomass smoke chamber experiments from the nascent smoke following the injection of ozone at t = 0, but exhibited a wide degree of variability. We show in Figure 2a the concentration of N_2O_5 formed during various experiments using authentic smoke or ammonium bisulfate control aerosol. The formation of N_2O_5 in a biomass-burning plume is not necessarily a given. If there is sufficient ozone in excess of NO, the NO_3 radical produced by reaction of O_3 with NO_x can also react rapidly with volatile organic compounds (VOCs), which are abundant in biomass-burning plumes[19] and may out-compete reaction with NO_2 (R2), and thus limit the formation of N_2O_5. However, for similar amounts of O_3 and NO_x, a similar amount of N_2O_5 was produced for both ammonium bisulfate experiments, which were devoid of volatile organic compounds. N_2O_5 production does not appear to be impeded by the presence of the organic vapors emitted in the smoke and transported through the eductor diluters to the chamber. Gas-phase organic nitrates detected by the UW-CIMS instrument did not support NO_3 reactions with VOCs to be a major sink (e.g. >20%) of N_2O_5 in these experiments. It is possible that efficient reaction of N_2O_5 on chamber walls was a major component of the NO_3 sink term, weakening a sensitivity to NO_3 chemistry.

Using the UW-CIMS we measured the maximum amount of N_2O_5 observed to vary by more than 60%, and also variation in the temporal trends of N_2O_5 formation and loss for different fuels and experiments (Figure 2a). This variability was likely due to different initial concentrations of NO_x and ozone in the chamber (listed in Table S1), variability in the organic vapors emitted, as well as the 10 minute mixing time associated with the 12 m^3 smog chamber volume. At t = ~0.5 hour, the N_2O_5 concentrations began to decrease for two likely reasons: 1) production of N_2O_5 decreases due to consumption of the precursors NO_x and O_3; 2) N_2O_5 is also being lost by uptake to the particles and chamber walls, where it may decompose and liberate NO_x, or be converted to either HNO_3 or $ClNO_2$ [75,76]. Different concentrations of particles present in the chamber will also affect the probability that a N_2O_5 molecule will collide with a particle versus the smog chamber wall.

If N_2O_5 is converted to $ClNO_2$ in the aerosol aqueous phase following reactive uptake, $ClNO_2$ rapidly partitions into the gas phase. Figure 2b shows the concentration of $ClNO_2$(g) measured by the UW-CIMS. $ClNO_2$ is stable in the dark smog chamber, and thus has no significant sinks in these experiments. As seen in Figure 2b, the concentration

of $ClNO_2$ only increases, unless the UV lights in the smog chamber are turned on. To illustrate the effect of the sunlight on the system, UV lights were turned on at t = 1 hour for a birch experiment, shown in Fig 2. The N_2O_5 photolyzes very rapidly, due to photolysis of NO_3 and its equilibrium with N_2O_5 (R3), but the $ClNO_2$ dissociates much slower. We confirmed the representativeness of the N_2O_5 traces shown in Figure 2 by injecting NO_2 and O_3 into the smog chamber without any particles; the N_2O_5 concentration had a similar temporal profile to the experiments with BBA. In all experiments N_2O_5 initially increased following the reaction of NO_x with O_3, and then gradually decreased while $ClNO_2$ increased.

Figure 2b shows that smoke from sawgrass (red) and cutgrass (green) generate more $ClNO_2$ than smoke from birch wood (purple) or ammonium bisulfate seed aerosol (black). We did observe the formation of $ClNO_2$ in nominally chloride-free control experiments: the ammonium bisulfate seeded experiments (Figure 2), and in aerosol-free experiments (not shown). This is presumably due to chloride that was already present on – or subsequently partitioned to – the smog chamber walls. The effect of injecting biomass-burning emissions resulted in a higher concentration of $ClNO_2$ being formed than what was observed when similar amounts of N_2O_5 precursors (NO_x + O_3) were injected in the control experiments (ammonium bisulfate aerosol or aerosol free) without biomass-burning emissions. This is apparent in Figure 3, where the ordinate axis shows the amount of $ClNO_2$ formed, normalized by the maximum N_2O_5 the was observed for a given experiment. The grey markers, representing ammonium bisulfate seeded experiments, are all lower than the other markers, representing the biomass burning experiments. The nominally chloride-free ammonium bisulfate experiment (maximum N_2O_5 = 1.05 ppbv) had a $ClNO_2$ concentration of 28 pptv after 1.7 hours, whereas the dry birch smoke experiment (maximum N_2O_5 = 1.06 ppbv) had 68 pptv of $ClNO_2$ after 1.7 hours.

In Figure 3 we plot the normalized, maximum $ClNO_2$ concentration observed as a function of *fCl*, the maximum (initial) particulate chloride non-refractory mass fraction. Using *fCl* reveals the effect of particle composition rather than the effect of total particle mass concentration on the production of $ClNO_2$. Furthermore, we normalized the maximum $ClNO_2$ by the maximum N_2O_5 observed to reduce the influence of simply having more $ClNO_2$ precursor available for reaction, caused by variability in the initial concentrations of NO_x, O_3, and VOCs (that scavenge NO_3) in the nascent smoke. As $ClNO_2$ has no sinks in the dark smog chamber, its maximum concentration is equivalent to the total $ClNO_2$ production. Figure 3 reveals a positive though weak correlation between initial particle chloride content and $ClNO_2$ produced. Given the variability in experimental conditions associated with biomass burning aerosol composition and emissions[19,53], the correlation across multiple fuels and relative humidity conditions is noteworthy. Normalizing by the maximum N_2O_5 shows a similar trend as using the time integrated N_2O_5, however changes in the sinks of N_2O_5 during an experiment (e.g. UV lights, adding water, particles, etc.) can change the integrated N_2O_5, after the majority of the $ClNO_2$ has been formed. Thus, for the best simplest comparison, we normalized the $ClNO_2$ by the maximum N_2O_5, which we believe best represents the N_2O_5 production, as

opposed to normalizing by the integrated N_2O_5 value which represents the sum of the N_2O_5 production and variable sinks.

Even aerosol systems with low-chloride content (*fCl* = 0.01), such as the birch-wood smoke, may result in an enhanced formation of $ClNO_2$ relative to what we observed from chloride-free aerosol experiments. With increasing *fCl*, there is an increase in $ClNO_2$ produced per N_2O_5 molecule available for reaction. For biomass burning experiments, a linear regression fit results in an $R^2 = 0.27$ ($ClNO_2/N_2O_{5\text{-max}} = 0.4*fCl + 0.067$). For this fit we have excluded experiments which did not have the requisite data due to lack of instrument availability, and one sawgrass experiment that had much lower particle surface area relative to other burns. Lack of particle surface area may result in an increased effect of N_2O_5 interacting with the chamber walls, instead of the smoke particles. With this analysis, we have directly demonstrated in the laboratory that biomass-burning plumes may be a source of both atmospheric N_2O_5 and $ClNO_2$, and that the efficacy with which N_2O_5 is converted to $ClNO_2$ is correlated with the particulate chloride mass fraction, *fCl*.

One limitation of smog chamber experiments is the potential for reactants to interact with the smog chamber walls. In an ideal experiment, N_2O_5 would only be lost by thermolysis (R3) or by reactive uptake on the particles (R4), as occurs in the atmosphere. This would allow us to directly calculate γ_{N2O5} of the BBA using just the measured particle surface area and loss rate of N_2O_5(g). An accurate measurement of γ_{N2O5} would in turn allow for a precise calculation of φ_{ClNO2} from the observed increase in $ClNO_2$(g). However, for our experimental conditions it appears that the loss of N_2O_5 was strongly influenced by interactions with the chamber walls. We confirmed this by injecting NO_2 and O_3 into the smog chamber without any particles; the N_2O_5 concentration had a similar temporal profile to the experiments with BBA. From this we conclude that the N_2O_5 was diffusing to the walls and being taken up with some efficiency, which in turn may produce some $ClNO_2$ from whatever chloride salts exist on the smog chamber walls from past experiments. While the aerosol-free experiments and ammonium bisulfate experiments do allow us to calculate the γ_{N2O5} and φ_{ClNO2} for reactions of N_2O_5 with the chamber walls, to do so requires detailed modeling of the gas-phase kinetics and turbulent transfer to the chamber walls. This will be the subject of a future manuscript. Here we draw some conclusions about γ_{N2O5} and φ_{ClNO2} by comparing with the ammonium bisulfate experiments, for which these heterogeneous kinetics have been well-characterized[7,25,69].

We compare the evolution of N_2O_5 and $ClNO_2$ for the BBA smoke experiments to the experiments where deliquesced ammonium bisulfate aerosol was injected into the smog chamber. In Figure 2a the ammonium bisulfate experiments are shown in grey, and we see that for a similar particle surface area as the biomass burning experiments, there is a much faster N_2O_5 decay at t = 0.4 hours. We do not differentiate between humidified and non-humidified biomass-burning aerosol for this comparison because in both cases the γ_{N2O5} for the biomass burning experiments must be much smaller than that known for the deliquesced ammonium bisulfate ($\gamma_{N2O5} = 0.03$[69]), otherwise we would see a similarly fast decay in those experiments. The reactive uptake of N_2O_5 on BBA is likely 1-2 orders of magnitude lower than on NH_4HSO_4(aq), similar to that observed for secondary organic

aerosol proxies (1.5×10^{-4})[25,29]. Humidification of the BBA did not significantly accelerate the reactive uptake of N_2O_5, even though particulate water content is an important driver of γ_{N2O5} based on prior studies using inorganic and organic aerosol particles.[7,25,28] BBA contains organic compounds that may inhibit reactive uptake of N_2O_5 by reducing the availability of water at the gas-particle interface, but also contains significant amounts of hygroscopic inorganic salts (such as KCl and NH_4Cl, and nitrates) whose associated water content would facilitate the uptake of N_2O_5 and formation of $ClNO_2$. The inferred small γ_{N2O5} also confirms that the φ_{ClNO2} of the BBA may be significant given that the absolute $ClNO_2$ concentration increases significantly over the ammonium bisulfate experiments, despite fewer molecules of N_2O_5 being taken up per collision by the BBA compared to the ammonium bisulfate.

3.3. Chloride displacement by nitric acid in BBA

We explored the effect of relative humidity, and thereby particulate water concentration, on the uptake of N_2O_5 and production of $ClNO_2$ by BBA. Although an aqueous phase is necessary to produce $ClNO_2$, water uptake will also reduce the concentration of chloride in the particles. This can favor the production of HNO_3 (R6) versus $ClNO_2$ (R7) through N_2O_5 hydrolysis as the Cl^- reactant and the nitrate effect (R5) are both diluted[7].

Figure 4 shows the effect of injecting steam into the smog chamber on particle composition. Starting at t = 0.6 hours, particulate chloride decreased as we increased the relative humidity. However, we saw no change in the rate of $ClNO_2$ formation, and thus we believe we are observing a rapid hydrochloric acid displacement reaction (R8). This would explain the rapid loss of chloride and increase of particulate nitrate without the subsequent enhanced production of $ClNO_2$. However, the N_2O_5 concentration did not decrease substantially in response to the particulate nitrate increase, which suggests that the displacement of HCl(g) was induced at least in part by another mechanism. Acid displacement of Cl^- as HCl(g) through uptake of the stronger acid HNO_3(g) directly, rather than by HNO_3(aq) generated through uptake of N_2O_5(g), is another chloride-nitrate substitution mechanism that was likely occurring[77–79]. It should be noted that in a biomass-burning plume, any displaced HCl(g) may still become neutralized by NH_3(g), which is also emitted from burning biomass, and condense as NH_4Cl [18,80–82]. This chloride would then again be available for heterogeneous displacement through uptake of N_2O_5 or HNO_3.

As shown in Figure 4, even a modest increase in relative humidity can cause a rapid increase in particulate nitrate and decrease in particulate chloride. Figure 5 shows the effect of a relative humidity ramp on the particulate chloride mass fraction, *fCl*. Markers are colored according to particle type, consistent with Figure 3. Marker symbols indicate if the reported measurement was taken before (hexagons) or after (bow ties) the steam injection. In some cases the smog chamber was pre-humidified, or steam was never injected, and thus for those two cases both markers for the same experiment will be at the same RH. Cutgrass and sawgrass both saw significant, but incomplete, reductions in particulate chloride. After humidification, between 40 and 76% of particulate chloride was displaced into the gas-phase. We also observed that a higher *fCl* prior to acid

displacement resulted in a higher *fCl* following acid displacement. For example, two experiments, one with sawgrass smoke and the other with cutgrass smoke, started with an initial *fCl* = 0.110 ± 0.005 and after humidification decreased to a final *fCl* = 0.037 ± 0.007. However, a birch burn that began with an initial *fCl* = 0.009 decreased after humidification to *fCl* = 0.006. Although in both cases the reduction in *fCl* was about 60% of the initial value, the remaining particulate Cl appears to still be active for $ClNO_2$ production, as indicated by experiments that were pre-humidified ("wet" in Figure 3).

We investigated a relative humidity of up to 60%, but we did not observe any further chloride displacement beyond what was observed at 10% RH. This incomplete displacement of Cl^- suggests that the displacement was limited by the availability of HNO_3(g or aq) that forms in the smoke aerosol. An alternate explanation is that the Cl^- that was not displaced was effectively encapsulated by black carbon or other particulate components, and therefore not available for reaction. However, if this Cl^- was unavailable for acid displacement by HNO_3, then it would also be unavailable for $ClNO_2$ formation. $ClNO_2$ formation appears to be consistent with the observed particulate Cl^- content, regardless of whether it has undergone acid displacement (Figure 5). The triangle markers in Figure 3 indicate experiments where the particles were humidified before $ClNO_2$ formation. These markers follow the same trend, increasing $ClNO_2/N_2O_{5\text{-max}}$ with increasing *fCl*, as other low-*fCl* aerosol systems, independent of relative humidity. This demonstrates that after acid displacement, the nitrate effect is not strongly inhibiting N_2O_5 uptake, and that although some of the particulate chloride does not become displaced by HNO_3, it is still available for the formation of $ClNO_2$. AMS measurements of particle composition show that the change in moles of chloride versus the change in moles of nitrate is -0.89 ± 0.42 (Figure S1). For reference, the stoichiometry of reaction R8 would result in a slope of -1.

Now that we have confirmed that N_2O_5 and $ClNO_2$ can be readily produced under nocturnal conditions in biomass-burning plumes with the addition of ozone, despite the competing nitrate radical loss by VOCs and chloride loss by acid displacement, future work will focus on kinetic modeling to quantify the N_2O_5 wall loss in these experiments. This will enable the calculation of the reactive uptake probability of N_2O_5 (γ_{N2O5}) and the yield of $ClNO_2$ (φ_{ClNO2}) for the biomass-burning aerosols we tested, and how these vary with particle composition and relative humidity. These are the key parameters that have previously been implemented in chemical transport models to study the impact of N_2O_5 uptake and chlorine activation chemistry on the atmospheric oxidant budget. These models can then be used to estimate the impact of the N_2O_5 and $ClNO_2$ formation that, based on these new findings, are likely to occur substantially during nocturnal processing of biomass-burning plumes[83,84].

Acknowledgements. This research was supported by the National Science Foundation (AGS-1551981 & AGS-1552608). LJ was partially supported by a Steinbrenner Fellowship from Carnegie Mellon University. We thank Robert Askins and Bert Wyatt at the Savannah National Wildlife Refuge for providing the authentic grass fuel samples for this study.

Supporting Information. Includes additional details for experimental methods and data analysis protocols, a summary table of experimental conditions, and one additional figure of results.

References

(1) Dentener, F. J.; Crutzen, P. J. Reaction of N2O5 on tropospheric aerosols: Impact on the global distributions of NOx , O3 , and OH. *J. Geophys. Res. Atmos.* **1993**, *98* (D4), 7149–7163.

(2) Brown, S. S.; Ryerson, T. B.; Wollny, A. G.; Brock, C. A.; Peltier, R.; Sullivan, A. P.; Weber, R. J.; Dube, W. P.; Trainer, M.; Meagher, J. F.; et al. Variability in nocturnal nitrogen oxide processing and its role in regional air quality. *Science (80-.).* **2006**, *311* (5757), 67–70.

(3) Atkinson, R.; Baulch, D. L.; Cox, R. A.; Crowley, J. N.; Hampson, R. F.; Hynes, R. G.; Jenkin, M. E.; Rossi, M. J.; Troe, J. Evaluated kinetic and photochemical data for atmospheric chemistry: Volume I - gas phase reactions of O_x, HO_x, NO_x and SO_x species. *Atmos. Chem. Phys.* **2004**, *4* (6), 1461–1738.

(4) Cox, R. A.; Derwent, R. G. The ultraviolet absorption spectrum of gaseous nitrous acid. *J. Photochem.* **1976**, *6*, 23–24.

(5) Hecht, T. A.; Seinfeld, J. H. Development and validation of a generalized mechanism for photochemical smog. *Environ. Sci. Technol.* **1972**, *6* (1), 47–57.

(6) Chang, W. L.; Bhave, P. V; Brown, S. S.; Riemer, N.; Stutz, J.; Dabdub, D. Heterogeneous Atmospheric Chemistry, Ambient Measurements, and Model Calculations of N2O5 : A Review. *Aerosol Sci. Technol.* **2011**, *45* (6), 665–695.

(7) Bertram, T. H.; Thornton, J. A. Toward a general parameterization of N_2O_5 reactivity on aqueous particles: the competing effects of particle liquid water, nitrate and chloride. *Atmos. Chem. Phys.* **2009**, *9* (21), 8351–8363.

(8) Behnke, W.; George, C.; Scheer, V.; Zetzsch, C. Production and decay of ClNO2 from the reaction of gaseous N205 with NaCl solution : Bulk and aerosol experiments. *J. Geophys. Res.* **1997**, *102* (D3), 3795–3804.

(9) Finlayson-Pitts, B. J.; Ezell, M. J.; Pitts, J. N. Formation of chemically active chlorine compounds by reactions of atmospheric NaCl particles with gaseous N2O5 and ClONO2. *Nature* **1989**, *337* (6204), 241–244.

(10) Young, C. J.; Washenfelder, R. A.; Roberts, J. M.; Mielke, L. H.; Osthoff, H. D.; Tsai, C.; Pikelnaya, O.; Stutz, J.; Veres, P. R.; Cochran, A. K.; et al. Vertically resolved measurements of nighttime radical reservoirs in los angeles and their contribution to the urban radical budget. *Environ. Sci. Technol.* **2012**, *46* (20), 10965–10973.

(11) Osthoff, H. D.; Roberts, J. M.; Ravishankara, A. R.; Williams, E. J.; Lerner, B. M.;

Sommariva, R.; Bates, T. S.; Coffman, D.; Quinn, P. K.; Dibb, J. E.; et al. High levels of nitryl chloride in the polluted subtropical marine boundary layer. *Nat. Geosci.* **2008**, *1* (5), 324–328.

(12) Mielke, L. H.; Stutz, J.; Tsai, C.; Hurlock, S. C.; Roberts, J. M.; Veres, P. R.; Froyd, K. D.; Hayes, P. L.; Cubison, M. J.; Jimenez, J. L.; et al. Heterogeneous formation of nitryl chloride and its role as a nocturnal NO x reservoir species during CalNex-LA 2010. *J. Geophys. Res. Atmos.* **2013**, *118* (18), 10,638-10,652.

(13) Thornton, J. A.; Kercher, J. P.; Riedel, T. P.; Wagner, N. L.; Cozic, J.; Holloway, J. S.; Dubé, W. P.; Wolfe, G. M.; Quinn, P. K.; Middlebrook, A. M.; et al. A large atomic chlorine source inferred from mid-continental reactive nitrogen chemistry. *Nature* **2010**, *464* (7286), 271–274.

(14) Wang, T.; Tham, Y. J.; Xue, L.; Li, Q.; Zha, Q.; Wang, Z.; Poon, S. C. N.; Dubé, W. P.; Blake, D. R.; Louie, P. K. K.; et al. Observations of nitryl chloride and modeling its source and effect on ozone in the planetary boundary layer of southern China. *J. Geophys. Res. Atmos.* **2016**, *121* (5), 2476–2489.

(15) Tham, Y. J.; Wang, Z.; Li, Q.; Yun, H.; Wang, W.; Wang, X.; Xue, L.; Lu, K.; Ma, N.; Bohn, B.; et al. Significant concentrations of nitryl chloride sustained in the morning: investigations of the causes and impacts on ozone production in a polluted region of northern China. *Atmos. Chem. Phys.* **2016**, *16* (23), 14959–14977.

(16) Brown, S. S.; Dubé, W. P.; Tham, Y. J.; Zha, Q.; Xue, L.; Poon, S.; Wang, Z.; Blake, D. R.; Tsui, W.; Parrish, D. D.; et al. Nighttime chemistry at a high altitude site above Hong Kong. *J. Geophys. Res. Atmos.* **2016**, *121* (5), 2457–2475.

(17) Mielke, L. H.; Furgeson, A.; Odame-Ankrah, C. A.; Osthoff, H. D. Ubiquity of $ClNO_2$ in the urban boundary layer of Calgary, Alberta, Canada. *Can. J. Chem.* **2016**, *94* (4), 414–423.

(18) Levin, E. J. T.; McMeeking, G. R.; Carrico, C. M.; Mack, L. E.; Kreidenweis, S. M.; Wold, C. E.; Moosmüller, H.; Arnott, W. P.; Hao, W. M.; Collett, J. L.; et al. Biomass burning smoke aerosol properties measured during Fire Laboratory at Missoula Experiments (FLAME). *J. Geophys. Res. - Atmos.* **2010**, *115*, D18210.

(19) Stockwell, C. E.; Yokelson, R. J.; Kreidenweis, S. M.; Robinson, A. L.; DeMott, P. J.; Sullivan, R. C.; Reardon, J.; Ryan, K. C.; Griffith, D. W. T.; Stevens, L. Trace gas emissions from combustion of peat, crop residue, domestic biofuels, grasses, and other fuels: configuration and Fourier transform infrared (FTIR) component of the fourth Fire Lab at Missoula Experiment (FLAME-4). *Atmos. Chem. Phys.* **2014**, *14* (18), 9727–9754.

(20) Lobert, J. M.; Keene, W. C.; Logan, J. A.; Yevich, R. Global chlorine emissions from biomass burning: Reactive Chlorine Emissions Inventory. *J. Geophys. Res. Atmos.* **1999**, *104* (D7), 8373–8389.

(21) Schlosser, J. S.; Braun, R. A.; Bradley, T.; Dadashazar, H.; MacDonald, A. B.; Aldhaif, A. A.; Aghdam, M. A.; Mardi, A. H.; Xian, P.; Sorooshian, A. Analysis of aerosol composition data for western United States wildfires between 2005 and 2015: Dust emissions, chloride depletion, and most enhanced aerosol constituents. *J. Geophys. Res. Atmos.* **2017**, *122* (16), 8951–8966.

(22) Alexander, B. Impact of preindustrial biomass-burning emissions on the oxidation pathways of tropospheric sulfur and nitrogen. *J. Geophys. Res.* **2004**, *109* (D8), D08303.

(23) Riedel, T. P.; Wagner, N. L.; Dubé, W. P.; Middlebrook, A. M.; Young, C. J.; Öztürk, F.; Bahreini, R.; VandenBoer, T. C.; Wolfe, D. E.; Williams, E. J.; et al. Chlorine activation within urban or power plant plumes: Vertically resolved ClNO2 and Cl2 measurements from a tall tower in a polluted continental setting. *J. Geophys. Res. Atmos.* **2013**, *118* (15), 8702–8715.

(24) Graedel, T. E.; Keene, W. C. Tropospheric budget of reactive chlorine. *Global Biogeochem. Cycles* **1995**, *9* (1), 47–77.

(25) Abbatt, J. P. D.; Lee, A. K. Y.; Thornton, J. A. Quantifying trace gas uptake to tropospheric aerosol: recent advances and remaining challenges. *Chem. Soc. Rev.* **2012**, *41* (19), 6555–6581.

(26) McNeill, V. F.; Patterson, J.; Wolfe, G. M.; Thornton, J. A. The effect of varying levels of surfactant on the reactive uptake of N2O5 to aqueous aerosol. *Atmos. Chem. Phys.* **2006**, *6*, 1635–1644.

(27) Ryder, O. S.; Campbell, N. R.; Morris, H.; Forestieri, S.; Ruppel, M. J.; Cappa, C.; Tivanski, A.; Prather, K.; Bertram, T. H. Role of Organic Coatings in Regulating N_2O_5 Reactive Uptake to Sea Spray Aerosol. *J. Phys. Chem. A* **2015**, *119* (48), 11683–11692.

(28) Gaston, C. J.; Thornton, J. A.; Ng, N. L. Reactive uptake of N2O5 to internally mixed inorganic and organic particles: The role of organic carbon oxidation state and inferred organic phase separations. *Atmos. Chem. Phys.* **2014**, *14* (11), 5693–5707.

(29) Escorcia, E. N.; Sjostedt, S. J.; Abbatt, J. P. D. Kinetics of N 2 O 5 Hydrolysis on Secondary Organic Aerosol and Mixed Ammonium Bisulfate−Secondary Organic Aerosol Particles. *J. Phys. Chem. A* **2010**, *114* (50), 13113–13121.

(30) McNeill, V. F.; Patterson, J.; Wolfe, G. M.; Thornton, J. A. The effect of varying levels of surfactant on the reactive uptake of N_2O_5 to aqueous aerosol. *Atmos. Chem. Phys.* **2006**, *6* (6), 1635–1644.

(31) Thornton, J. A.; Braban, C. F.; Abbatt, J. P. D. N2O5 hydrolysis on sub-micron organic aerosols: the effect of relative humidity, particle phase, and particle size. *Physical Chemistry Chemical Physics*. 2003, p 4593.

(32) Knopf, D. A.; Forrester, S. M.; Slade, J. H. Heterogeneous oxidation kinetics of organic biomass burning aerosol surrogates by O3, NO2, N2O5, and NO3. *Phys. Chem. Chem. Phys.* **2011**, *13* (47), 21050.

(33) Reid, J. S.; Koppmann, R.; Eck, T. F.; Eleuterio, D. P. A review of biomass burning emissions part II: intensive physical properties of biomass burning particles. *Atmos. Chem. Phys.* **2005**, *5*, 799–825.

(34) Akagi, S. K.; Craven, J. S.; Taylor, J. W.; McMeeking, G. R.; Yokelson, R. J.; Burling, I. R.; Urbanski, S. P.; Wold, C. E.; Seinfeld, J. H.; Coe, H.; et al. Evolution of trace gases and particles emitted by a chaparral fire in California. *Atmos. Chem. Phys.* **2012**, *12* (3), 1397–1421.

(35) Alvarado, M. J.; Lonsdale, C. R.; Yokelson, R. J.; Akagi, S. K.; Coe, H.; Craven, J. S.; Fischer, E. V.; McMeeking, G. R.; Seinfeld, J. H.; Soni, T.; et al. Investigating the links between ozone and organic aerosol chemistry in a biomass burning plume from a prescribed fire in California chaparral. *Atmos. Chem. Phys.* **2015**, *15* (12), 6667–6688.

(36) Yokelson, R. J.; Crounse, J. D.; DeCarlo, P. F.; Karl, T.; Urbanski, S.; Atlas, E.; Campos, T.; Shinozuka, Y.; Kapustin, V.; Clarke, A. D.; et al. Emissions from biomass burning in the Yucatan. *Atmos. Chem. Phys.* **2009**, *9* (15), 5785–5812.

(37) Li, J.; Pósfai, M.; Hobbs, P. V.; Buseck, P. R. Individual aerosol particles from biomass burning in southern Africa: 2, Compositions and aging of inorganic particles. *J. Geophys. Res. Atmos.* **2003**, *108* (D13), doi: 10.1029/2002JD002310.

(38) Roberts, J. M.; Osthoff, H. D.; Brown, S. S.; Ravishankara, A. R.; Coffman, D.; Quinn, P.; Bates, T. Laboratory studies of products of N_2O_5 uptake on Cl^- containing substrates. *Geophys. Res. Lett.* **2009**, *36* (20), L20808.

(39) Kercher, J. P.; Riedel, T. P.; Thornton, J. A. Chlorine activation by N2O5: simultaneous, in situ detection of ClNO2 and N2O5 by chemical ionization mass spectrometry. *Atmos. Meas. Tech.* **2009**, *2* (1), 193–204.

(40) Roberts, J. The atmospheric chemistry of organic nitrates. *Atmos. Environ. Part A. Gen. Top.* **1990**, *24* (2), 243–287.

(41) Mentel, T. F.; Sohn, M.; Wahner, A. Nitrate effect in the heterogeneous hydrolysis of dinitrogen pentoxide on aqueous aerosols. *Phys. Chem. Chem. Phys.* **1999**, *1* (24), 5451–5457.

(42) Hu, J. H.; Abbatt, J. P. D. Reaction probabilities for N2O5 hydrolysis on sulfuric acid and ammonium sulfate aerosols at room temperature. *J. Phys. Chem. A* **1997**, *101* (5), 871–878.

(43) Bertram, A. K.; Martin, S. T.; Hanna, S. J.; Smith, M. L.; Bodsworth, A.; Chen, Q.; Kuwata, M.; Liu, A.; You, Y.; Zorn, S. R. Predicting the relative humidities of liquid-

liquid phase separation, efflorescence, and deliquescence of mixed particles of ammonium sulfate, organic material, and water using the organic-to-sulfate mass ratio of the particle and the oxygen-to-carbon elemental ratio of the organic component. *Atmos. Chem. Phys.* **2011**, *11* (21), 10995–11006.

(44) Ciobanu, V. G.; Marcolli, C.; Krieger, U. K.; Weers, U.; Peter, T. Liquid−Liquid Phase Separation in Mixed Organic/Inorganic Aerosol Particles. *J. Phys. Chem. A* **2009**, *113* (41), 10966–10978.

(45) Gorkowski, K.; Beydoun, H.; Aboff, M.; Walker, J. S.; Reid, J. P.; Sullivan, R. C. Advanced aerosol optical tweezers chamber design to facilitate phase-separation and equilibration timescale experiments on complex droplets. *Aerosol Sci. Technol.* **2016**, *50* (12), 1327–1341.

(46) Renbaum-Wolff, L.; Song, M.; Marcolli, C.; Zhang, Y.; Liu, P. F.; Grayson, J. W.; Geiger, F. M.; Martin, S. T.; Bertram, A. K. Observations and implications of liquid–liquid phase separation at high relative humidities in secondary organic material produced by *a*-pinene ozonolysis without inorganic salts. *Atmos. Chem. Phys.* **2016**, *16* (12), 7969–7979.

(47) Gorkowski, K.; Donahue, N. M.; Sullivan, R. C. Emulsified and Liquid–Liquid Phase-Separated States of α-Pinene Secondary Organic Aerosol Determined Using Aerosol Optical Tweezers. *Environ. Sci. Technol.* **2017**, *51* (21), 12154–12163.

(48) Gard, E. E.; Kleeman, M. J.; Gross, D. S.; Hughes, L. S.; Allen, J. O.; Morrical, B. D.; Fergenson, D. P.; Dienes, T.; Galli, M. E.; Johnson, R. J.; et al. Direct observation of heterogeneous chemistry in the atmosphere. *Science* **1998**, *279* (5354), 1184–1187.

(49) Grieshop, A. P.; Donahue, N. M.; Robinson, A. L. Laboratory investigation of photochemical oxidation of organic aerosol from wood fires 2: analysis of aerosol mass spectrometer data. *Atmos. Chem. Phys.* **2009**, *9* (6), 2227–2240.

(50) Hennigan, C. J.; Sullivan, A. P.; Collett, J. L.; Robinson, A. L. Levoglucosan stability in biomass burning particles exposed to hydroxyl radicals. *Geophys. Res. Lett.* **2010**, *37*, L09806.

(51) Keene, W. C.; Lobert, R. M.; Crutzen, P. J.; Maben, J. R.; Scharffe, D. H.; Landmann, T.; Hely, C.; Brain, C. Emissions of major gaseous and particulate species during experimental burns of southern African biomass. *J. Geophys. Res.* **2006**, *111* (D4), D04301.

(52) Wade, D.; Ewel, J.; Hofstetter, R. *Fire In South Florida Ecosystems*; 1980; Vol. 17.

(53) Tkacik, D. S.; Robinson, E. S.; Ahern, A.; Saleh, R.; Stockwell, C.; Veres, P.; Simpson, I. J.; Meinardi, S.; Blake, D. R.; Yokelson, R. J.; et al. A dual-chamber method for quantifying the effects of atmospheric perturbations on secondary organic aerosol formation from biomass burning emissions. *J. Geophys. Res. Atmos.* **2017**, *122* (11),

6043–6058.

(54) Robinson, E. S.; Donahue, N. M.; Ahern, A. T.; Ye, Q.; Lipsky, E. Single-particle measurements of phase partitioning between primary and secondary organic aerosols. *Faraday Discuss.* **2016**, *189* (0), 31–49.

(55) Onasch, T. B.; Trimborn, A.; Fortner, E. C.; Jayne, J. T.; Kok, G. L.; Williams, L. R.; Davidovits, P.; Worsnop, D. R. Soot Particle Aerosol Mass Spectrometer: Development, Validation, and Initial Application. *Aerosol Sci. Technol.* **2012**, *46* (7), 804–817.

(56) Willis, M. D.; Lee, A. K. Y.; Onasch, T. B.; Fortner, E. C.; Williams, L. R.; Lambe, A. T.; Worsnop, D. R.; Abbatt, J. P. D. Collection efficiency of the soot-particle aerosol mass spectrometer (SP-AMS) for internally mixed particulate black carbon. *Atmos. Meas. Tech.* **2014**, *7* (12), 4507–4516.

(57) Ahern, A. T.; Subramanian, R.; Saliba, G.; Lipsky, E. M.; Donahue, N. M.; Sullivan, R. C. Effect of secondary organic aerosol coating thickness on the real-time detection and characterization of biomass-burning soot by two particle mass spectrometers. *Atmos. Meas. Tech.* **2016**, *9* (12), 6117–6137.

(58) DeCarlo, P. F.; Kimmel, J. R.; Trimborn, A.; Northway, M. J.; Jayne, J. T.; Aiken, A. C.; Gonin, M.; Fuhrer, K.; Horvath, T.; Docherty, K. S.; et al. Field-deployable, high-resolution, time-of-flight aerosol mass spectrometer. *Anal. Chem.* **2006**, *78* (24), 8281–8289.

(59) Jayne, J. T.; Leard, D. C.; Zhang, X.; Davidovits, P.; Smith, K. A.; Kolb, C. E.; Worsnop, D. R. Development of an Aerosol Mass Spectrometer for Size and Composition Analysis of Submicron Particles. *Aerosol Sci. Technol.* **2000**, *33* (1–2), 49–70.

(60) Carbone, S.; Onasch, T.; Saarikoski, S.; Timonen, H.; Saarnio, K.; Sueper, D.; Rönkkö, T.; Pirjola, L.; Häyrinen, A.; Worsnop, D.; et al. Characterization of trace metals on soot aerosol particles with the SP-AMS: detection and quantification. *Atmos. Meas. Tech.* **2015**, *8* (11), 4803–4815.

(61) Li, J.; Posfai, M.; Hobbs, P. V.; Buseck, P. R.; Pósfai, M.; Hobbs, P. V.; Buseck, P. R. Individual aerosol particles from biomass burning in southern Africa: 2, Compositions and aging of inorganic particles. *J. Geophys. Res. - Atmos.* **2003**, *108* (D13), doi: 10.1029/2002JD002310.

(62) Robinson, E. S.; Onasch, T. B.; Worsnop, D.; Donahue, N. M. Collection efficiency of alpha-pinene secondary organic aerosol particles explored via light scattering single particle aerosol mass spectrometry. *Atmos. Meas. Tech.* **2016**, 1–29.

(63) Docherty, K. S.; Jaoui, M.; Corse, E.; Jimenez, J. L.; Offenberg, J. H.; Lewandowski, M.; Kleindienst, T. E. Collection Efficiency of the Aerosol Mass Spectrometer for

Chamber-Generated Secondary Organic Aerosols. *Aerosol Sci. Technol.* **2013**, *47* (3), 294–309.

(64) Winer, A. M.; Peters, J. W.; Smith, J. P.; Pitts, J. N. Response of commercial chemiluminescent nitric oxide-nitrogen dioxide analyzers to other nitrogen-containing compounds. *Environ. Sci. Technol.* **1974**, *8* (13), 1118–1121.

(65) Villena, G.; Bejan, I.; Kurtenbach, R.; Wiesen, P.; Kleffmann, J. Interferences of commercial NO_2 instruments in the urban atmosphere and in a smog chamber. *Atmos. Meas. Tech.* **2012**, *5* (1), 149–159.

(66) Lopez-Hilfiker, F. D.; Mohr, C.; Ehn, M.; Rubach, F.; Kleist, E.; Wildt, J.; Mentel, T. F.; Lutz, A.; Hallquist, M.; Worsnop, D.; et al. A novel method for online analysis of gas and particle composition: description and evaluation of a Filter Inlet for Gases and AEROsols (FIGAERO). *Atmos. Meas. Tech.* **2014**, *7* (4), 983–1001.

(67) Gaston, C. J.; Lopez-Hilfiker, F. D.; Whybrew, L. E.; Hadley, O.; McNair, F.; Gao, H.; Jaffe, D. A.; Thornton, J. A. Online molecular characterization of fine particulate matter in Port Angeles, WA: Evidence for a major impact from residential wood smoke. *Atmos. Environ.* **2016**, *138*, 99–107.

(68) Lee, B. H.; Lopez-Hilfiker, F. D.; Mohr, C.; Kurtén, T.; Worsnop, D. R.; Thornton, J. A. An Iodide-Adduct High-Resolution Time-of-Flight Chemical-Ionization Mass Spectrometer: Application to Atmospheric Inorganic and Organic Compounds. *Environ. Sci. Technol.* **2014**, *48* (11), 6309–6317.

(69) Bertram, T. H.; Thornton, J. A.; Riedel, T. P. An experimental technique for the direct measurement of N_2O_5 reactivity on ambient particles. *Atmos. Meas. Tech.* **2009**, *2* (1), 231–242.

(70) Lopez-Hilfiker, F. D.; Iyer, S.; Mohr, C.; Lee, B. H.; D'ambro, E. L.; Kurtén, T.; Thornton, J. A. Constraining the sensitivity of iodide adduct chemical ionization mass spectrometry to multifunctional organic molecules using the collision limit and thermodynamic stability of iodide ion adducts. *Atmos. Meas. Tech.* **2016**, *9* (4), 1505–1512.

(71) Huffman, J. A.; Ziemann, P. J.; Jayne, J. T.; Worsnop, D. R.; Jimenez, J. L.; Aiken, A.; Docherty, K.; Ulbrich, I.; Decarlo, P.; Kimmel, J.; et al. Development and Characterization of a Fast-Stepping/Scanning Thermodenuder for Chemically-Resolved Aerosol Volatility Measurements. *Aerosol Sci. Technol.* **2008**, *42*, 395–407.

(72) Schauer, J. J.; Kleeman, M. J.; Cass, G. R.; Simoneit, B. R. T. Measurement of Emissions from Air Pollution Sources. 3. C 1 −C 29 Organic Compounds from Fireplace Combustion of Wood. *Environ. Sci. Technol.* **2001**, *35* (9), 1716–1728.

(73) Hays, M. D.; Geron, C. D.; Linna, K. J.; Smith, N. D.; Schauer, J. J. Speciation of Gas-Phase and Fine Particle Emissions from Burning of Foliar Fuels. *Environ. Sci.*

Technol. **2002**, *36* (11), 2281–2295.

(74) Salcedo, D.; Onasch, T. B.; Dzepina, K.; Canagaratna, M. R.; Zhang, Q.; Huffman, J. A.; DeCarlo, P. F.; Jayne, J. T.; Mortimer, P.; Worsnop, D. R.; et al. Characterization of ambient aerosols in Mexico City during the MCMA-2003 campaign with Aerosol Mass Spectrometry: results from the CENICA Supersite. *Atmos. Chem. Phys.* **2006**, *6* (4), 925–946.

(75) Wahner, A.; Mentel, T. F.; Sohn, M.; Stier, J. Heterogeneous reaction of N2O5 on sodium nitrate aerosol. *J. Geophys. Res. Atmos.* **1998**, *103* (D23), 31103–31112.

(76) Wahner, A.; Mentel, T. F.; Sohn, M. Gas-phase reaction of N 2 O 5 with water vapor: Importance of heterogeneous hydrolysis of N 2 O 5 and surface desorption of HNO3 in a large Teflon chamber. *Geophys. Res. Lett.* **1998**, *25* (12), 2169–2172.

(77) Li, C.; Ma, Z.; Chen, J.; Wang, X.; Ye, X.; Wang, L.; Yang, X.; Kan, H.; Donaldson, D. J.; Mellouki, A. Evolution of biomass burning smoke particles in the dark. *Atmos. Environ.* **2015**, *120*, 244–252.

(78) Song, C. H.; Carmichael, G. R. Gas-particle partitioning of nitric acid modulated by alkaline aerosol. *J. Atmos. Chem.* **2001**, *40* (1), 1–22.

(79) Sullivan, R. C.; Guazzotti, S. A.; Sodeman, D. A.; Prather, K. A. Direct observations of the atmospheric processing of Asian mineral dust. *Atmos. Chem. Phys.* **2007**, *7* (5), 1213–1236.

(80) DeCarlo, P. F.; Dunlea, E. J.; Kimmel, J. R.; Aiken, A. C.; Sueper, D.; Crounse, J.; Wennberg, P. O.; Emmons, L.; Shinozuka, Y.; Clarke, A.; et al. Fast airborne aerosol size and chemistry measurements above Mexico City and Central Mexico during the MILAGRO campaign. *Atmos. Chem. Phys.* **2008**, *8* (14), 4027–4048.

(81) Stockwell, C. E.; Veres, P. R.; Williams, J.; Yokelson, R. J. Characterization of biomass burning emissions from cooking fires, peat, crop residue, and other fuels with high-resolution proton-transfer-reaction time-of-flight mass spectrometry. *Atmos. Chem. Phys.* **2015**, *15* (2), 845–865.

(82) Whitburn, S.; Van Damme, M.; Kaiser, J. W.; van der Werf, G. R.; Turquety, S.; Hurtmans, D.; Clarisse, L.; Clerbaux, C.; Coheur, P.-F. Ammonia emissions in tropical biomass burning regions: Comparison between satellite-derived emissions and bottom-up fire inventories. *Atmos. Environ.* **2015**, *121*, 42–54.

(83) Simon, H.; Kimura, Y.; McGaughey, G.; Allen, D. T.; Brown, S. S.; Osthoff, H. D.; Roberts, J. M.; Byun, D.; Lee, D. Modeling the impact of $ClNO_2$ on ozone formation in the Houston area. *J. Geophys. Res.* **2009**, *114* (D7), D00F03.

(84) Sarwar, G.; Simon, H.; Bhave, P.; Yarwood, G. Examining the impact of heterogeneous nitryl chloride production on air quality across the United States. *Atmos. Chem. Phys.* **2012**, *12* (14), 6455–6473.

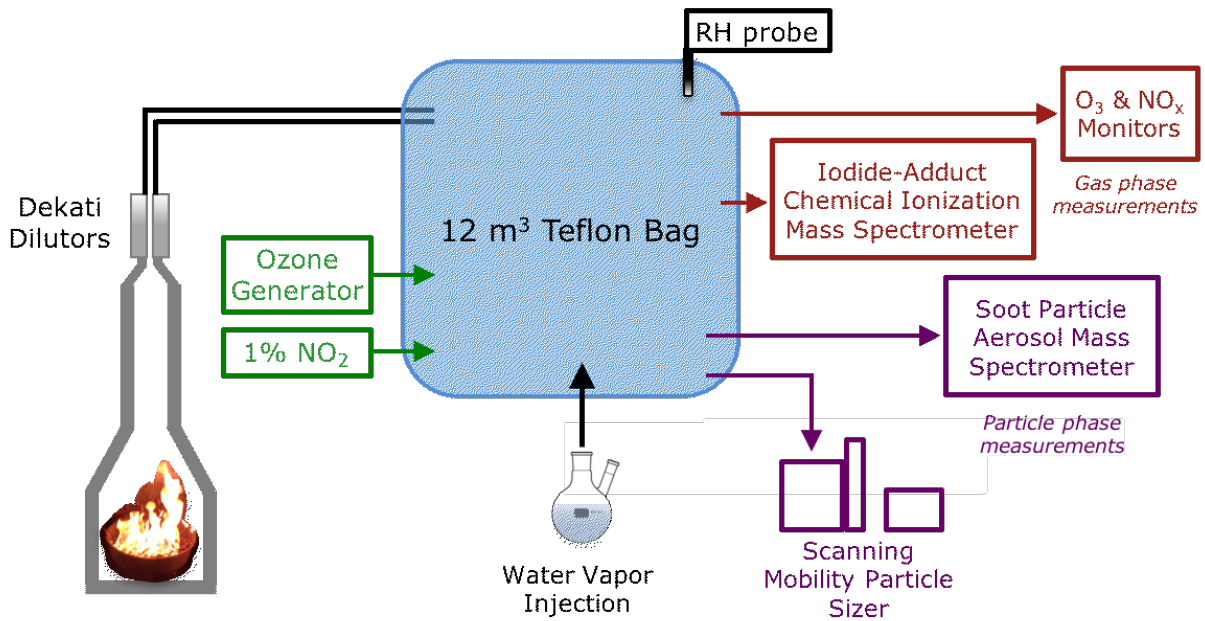

Figure 1. Experimental setup for biomass-burning aerosol smog chamber experiments. The CMU smog chamber was filled with precursors for N_2O_5 formation, either from biomass burning or from a compressed gas cylinder. Gas and particle phase instrumentation sampled air from the chamber reactor whose relative humidity was adjusted using steam. A high flow rate and short sampling line was used for the CIMS to reduce losses of reactants in the tubing.

749

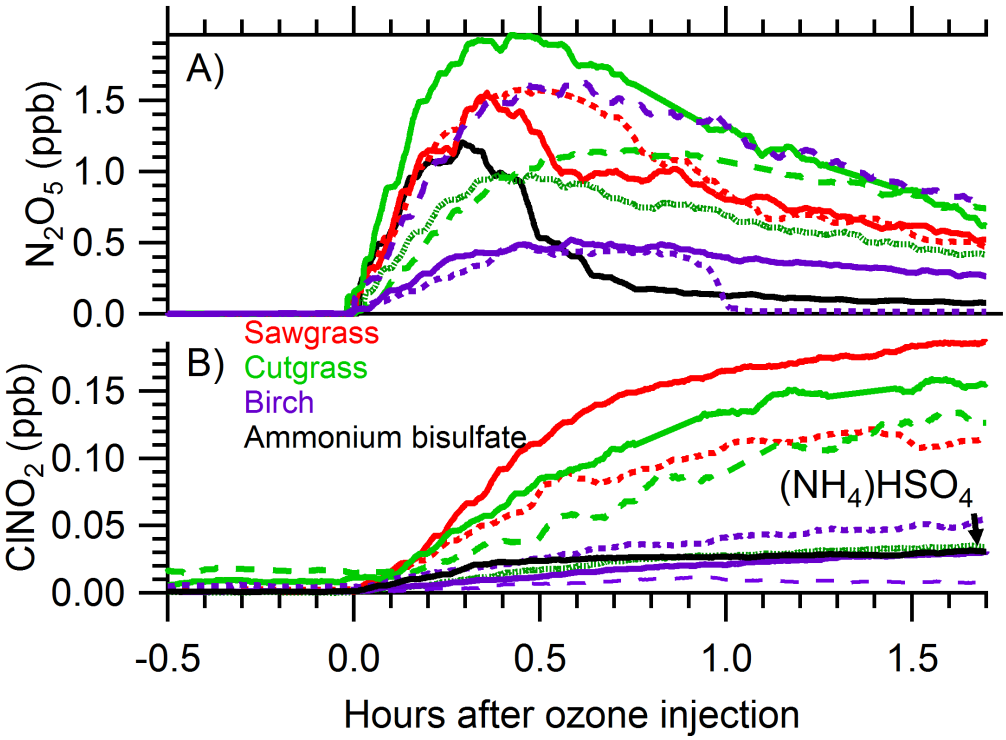

Figure 2. Production of N_2O_5(g) and $ClNO_2$(g), measured by the UW-CIMS, during dark chamber aging of biomass-burning aerosol or ammonium bisulfate control aerosol under varying RH conditions. Panel a) shows the formation of N_2O_5 for chamber experiments with different particle types. Panel b) shows the formation of $ClNO_2$. Grass burns appear to generate the most $ClNO_2$, but they also tend have the most N_2O_5 available to be converted. The trace color corresponds to the type of aerosol present, with replicate experiments of the same aerosol type shown by different line styles of the same color.

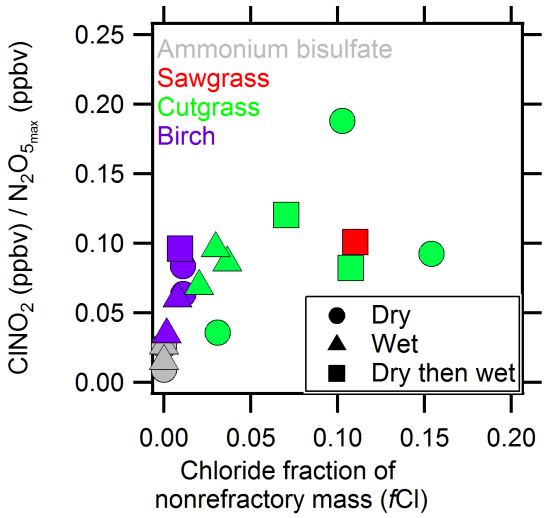

Figure 3. The ratio of the maximum concentration of $ClNO_2$(g) to the maximum concentration of N_2O_5(g) measured in each experiment, versus the chloride fraction of non-refractory particulate mass (*fCl*). The symbol shape corresponds to the relative humidity level in the chamber when the measurements were made. "Dry then wet" indicates that water vapor was injected into the initially dry chamber later in the experiment.

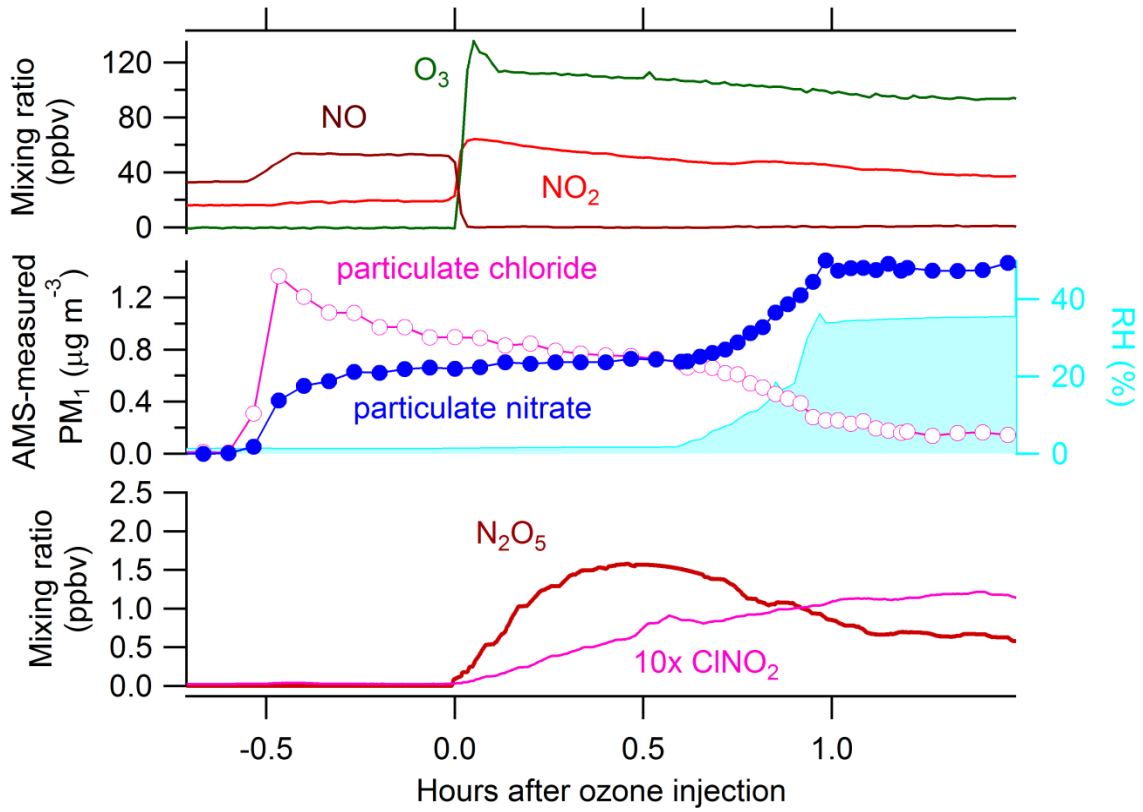

Figure 4. Gas and particle-phase time series for one exemplary biomass burning experiment using sawgrass where relative humidity was increased 30 minutes after O_3 had been injected into the smoke-filled chamber. The top panel shows the gas concentrations of O_3 and NO_2. The middle panel shows the mass concentrations of particulate nitrate and chloride measured by the SP-AMS, and the relative humidity (RH) in the chamber. The bottom panel shows the gas concentrations of N_2O_5 and $ClNO_2$ (x10) measured by the UW-CIMS.

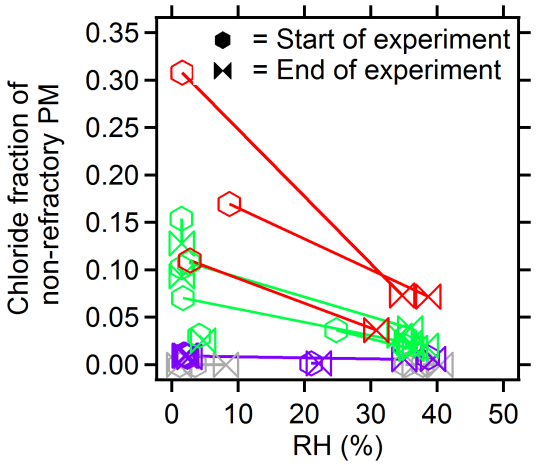

Figure 5. Chloride fraction of non-refractory particulate mass (*fCl*) as a function of chamber relative humidity. Hexagons indicate measurements taken at the beginning of the experiment, and bowties mark measurements at the end of the experiment. In some experiments steam was injected into the chamber to increase the relative humidity increase and *fCl* generally decreased. Color corresponds to the aerosol type present, as in Fig. 3.

750